Role of Hydrogen Bond Networks and Dynamics in Positive and Negative Cooperative Stabilization of a Protein†

Jasmina S. Redzic and Bruce E. Bowler*

Department of Chemistry and Biochemistry, 2190 East Iliff Avenue, University of Denver, Denver, Colorado 80208-2436

Received August 17, 2004; Revised Manuscript Received November 8, 2004

ABSTRACT: Cooperativity mediated through hydrogen bond networks in yeast iso-1-cytochrome *c* was studied using a thermodynamic triple mutant cycle. Three known stabilizing mutations, Asn 26 to His, Asn 52 to Ile, and Tyr 67 to Phe, were used to construct the triple mutant cycle. The side chain of His 26, a wild-type residue, forms two hydrogen bonds that bridge two substructures of the wild-type protein, and Tyr 67 and Asn 52 are part of an extensive buried hydrogen bond network. The stabilities of all variants in the triple mutant cycle were determined by guanidine hydrochloride denaturation methods and used to determine the pairwise, Δ^2G_{int}, and triple interaction energies. His 26 and Ile 52 interact cooperatively (Δ^2G_{int} is 1−2 kcal/mol), whereas the two other pairs of mutations interact anticooperatively (Δ^2G_{int} is −0.5 to −1.5 kcal/mol). Previously reported structural data for iso-1-cytochrome *c* variants containing these mutations show that changes in the strength of the His 26 to Glu 44 hydrogen bond, apparently caused by changes in main chain dynamics, provide a mechanism for the long distance (His 26 to Phe 67 and His 26 to Ile 52) propagation of pairwise interaction energies. Opposing changes in the strength of the His 26 to Glu 44 hydrogen bond caused by the N52I and Y67F mutations generate a negative triple interaction energy (−0.9 ±0.7 kcal/mol) that combined with cancellation of cooperative and anticooperative pairwise interactions produce apparent additivity for the stabilizing effects of the single mutations in the triple mutant variant.

Cytochrome *c* is known to have an extensive buried hydrogen bond network at the interface of several of its cooperative units. In particular, the least stable (nested subyellow or N-yellow) and second most stable (green) substructures contribute to this network (see Figure 1; refs *1* and *2*). To investigate the role of this hydrogen bond network in the cooperativity of cytochrome *c* folding, we have made mutations at residues in the N-yellow and green substructures that will disrupt the hydrogen bond network. We have used iso-1-cytchrome *c* from *Saccharomyces cerevisiae* for this purpose. Within the N-yellow substructure, we have mutated position 52 from an asparagine to an isoleucine (N52I),[1] and within the green substructure, we have mutated position 67 from a tyrosine to a phenylalanine (Y67F) to disrupt the buried hydrogen bond network. A third mutation at position 26 from asparagine to histidine (N26H) will also be investigated. In wild type (WT) iso-1-cytochrome *c*, position 26 is a histidine, it is in the green substructure, and its side chain makes two hydrogen bonds that bridge the N-yellow and green substructures (see Figure 1). From a thermodynamic perspective, we will be looking at the effect of introducing this native residue into iso-1-cytochrome *c*. Given the substructure bridging hydrogen bond of the His 26 side chain, these three mutation sites will also permit investigation of how changes in a buried hydrogen bond network impact a distant intersubstructural hydrogen bond (for distances between mutation sites, see Figure 1). In addition, these mutations were chosen because all are known to significantly stabilize iso-1-cytochrome *c* (*3*−*6*), and structural data is available for iso-1-cytochrome *c* variants containing each or both of the N52I and Y67F mutations, as well as for the WT protein (*7*−*9*).

As reported by Berghuis et al. (*7*), the N52I mutation brings about the displacement of the water 166 (Wat 166) molecule that seems to be a stabilizing factor in the oxidized form of the variant protein. The loss of Wat 166 also disrupts several hydrogen bonds: Wat 166 to Thr 78 side chain hydroxyl (OG1), Wat 166 to Tyr 67 (OH group), Wat 166 to Asn 52 side chain NH_2 (ND2), and Tyr 67 (OH) to Met 80 side chain sulfur (SD) (*7*, *8*). Because of the displacement of Wat 166, a new hydrogen bond is formed between the hydroxyl group of Tyr 67 and the side chain of Thr 78 (OG1). The hydrogen bond between Asn 52 (ND2) and the heme pyrrole A propionate (O2A) observed in the reduced state of iso-1-cytochrone *c* is not present in the oxidized state of the WT protein and has been associated with a large

† Acknowledgment is made to the donors of the Petroleum Research Fund (38865-AC4, B.E.B.) for support of this work. The Applied Photophysics PiStar 180 spectrometer was purchased with NIH Grant 1-510-RR16632-01.

* To whom correspondence should be addressed. Phone: (303) 871-2985. Fax: (303) 871-2254. E-mail: bbowler@du.edu.

[1] Abbreviations: CD, circular dichroism; AcTM, iso-1-cytochrome *c* variant (T(-5)S, K(-2)L, H26N, H33N, H39Q, C102S) that has been acetylated at the N-terminus to prevent it from binding to the heme under denaturing conditions as described in ref *13*; N52I, mutation of Asn 52 to Ile; Y67F, mutation of Tyr 67 to Phe; N26H, mutation of Asn 26 to His; AcH26, AcTM protein with the N26H mutation; AcI52, AcTM protein with the N52I mutation; AcF67, AcTM protein with the Y67F mutation; AcH26I52F67, AcTM protein with all three previously mentioned mutations; AcI52F67, AcTM variant with the N52I and Y67F mutations; AcH26I52, AcTM variant with the N26H and N52I mutations; AcH26F67, AcTM variant with the N26H and Y67F mutations; WT, wild-type protein; Wat 166, water molecule 166; Wat 300, water molecule 300; gdnHCl, guanidine hydrochloride.

10.1021/bi048218b CCC: $30.25
Published on Web 02/01/2005

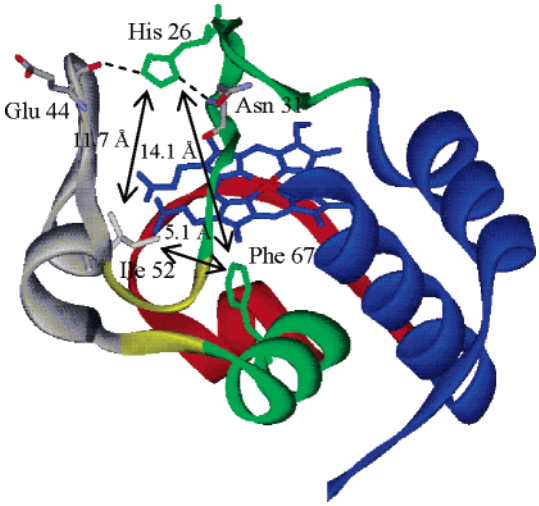

FIGURE 1: Yeast iso-1-cytochrome *c* in the oxidized state with the N52I and Y67F mutations, shown with the substructure classifications of horse cytochrome *c* according to refs *1* and *2*. The substructures are color coded gray (N-yellow, residues 40−57), red (residues 71−85), yellow (residues 37−39 and 58−61), green (60's helix and 20's-30's loop), and blue (N- and C-terminal helices), in the order of increasing stability. The amino acids, His 26, Ile 52, and Phe 67, are shown with stick models in the color of the substructure in which they are contained. Glu 44 and Asn 31, which participate in the intersubstructural hydrogen bond between the N-yellow and the green substructures, mediated by the side chain of His 26, are shown as stick models colored by element. Double-ended arrows are used to show the distances, in angstroms, of closest approach between the side chains of each residue in the triple mutant cycle. The distances are for the Y67F/N52I variant. In the pseudo-WT (C102T) structure, the distances of closest approach are similar, Asn 52 to His 26, 11.3 Å; Tyr 67 to His 26, 13.2 Å; and Asn 52 to Tyr 67, 5.6 Å (mediated via hydrogen bonds to water 166). The figure was prepared with DS ViewerPro software and the Protein Data Bank file 1CRI (*30*).

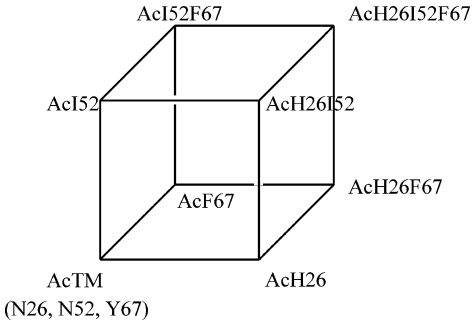

FIGURE 2: Triple mutant thermodynamic cycle used to investigate the energy of interaction among the double and triple mutant variants. The free energy of unfolding for each variant in the cycle was determined by gdnHCl denaturation methods monitored by circular dichroism. The double and triple interaction energies in the mutational cycle were determined using eqs 3−5 in Materials and Methods.

increase in the dynamics of the N-yellow substructure in the oxidized state (*8*). Although this hydrogen bond cannot be made in the N52I variant, an important effect of this mutation is that the large increase in dynamics of the N-yellow substructure observed upon oxidation of the WT protein (*8*) does not occur in the N52I variant (*7*).

Tyr 67 is also thought to be of structural importance to the WT protein; however, it is still unclear what role it actually plays (*9*). The mutation to a phenylalanine brings about several structural changes in the protein due to the loss of the hydroxyl group from the Tyr residue. The hydroxyl group is involved in the hydrogen bond network through interactions with the side chains of Asn 52 (ND2) and Met 80 (SD). As previously described by Berghuis et al. (*9*), there is no displacement of the Wat 166 as seen in the N52I protein, and the presence of another water molecule (Wat 300) is observed. The addition of the Wat 300 molecule rearranges the hydrogen bond network so that the only hydrogen bonds present are between Asn 52 (ND2) and heme propionate A (O2A), Thr 78 (OG1), and heme pyrrole D propionate (O2D) and Met 80 amide (ND) and Thr 78 (OG1). It is important to note that Wat 166 and Wat 300 are resolved in the reduced Y67F variant structure; however, they cannot be seen directly in the X-ray structure of the oxidized Y67F variant. They are presumed to be present but dynamically disordered (*9*). A key factor in this variant is that the Asn 52 (ND2) to heme propionate A hydrogen bond does not break in the oxidized Y67F protein as it does in the WT protein, causing the dynamics of the main chain to be significantly lower beyond residue 47 in the sequence. The double mutation involving these two residues, N52I/Y67F (*7*), brings about the displacement of the Wat 166 molecule and compression of the internal cavity to 8 $Å^3$ (too small for a H_2O molecule). The only hydrogen bond that remains in the buried hydrogen bond network is between the heme pyrrole D propionate (O1D) and Thr 78 (OG1).

From thermodynamic studies, it is known that the N26H, N52I, and Y67F mutations all stabilize iso-1-cytochrome *c* (*3*−*6*). In previous work, we also found a strong cooperative interaction between the N52I and N26H mutations (*6*). Since both the N52I and Y67F mutations affect the buried hydrogen bond network, it is of interest to determine whether the stabilization mechanisms of these two variants reinforce or interfere with each other. Similarly, it is of interest to determine whether cooperative interactions occur between the stabilizing Y67F mutation or the combined Y67F/N52I double mutation and the N26H mutation. Since position 26 is distant from positions 52 and 67 (Figure 1), such interactions would have to be propagated across a substantial distance.

The use of mutational thermodynamic cycles enables evaluation of the energy of interaction between side chains in a protein (*10*−*12*). To investigate the importance of the buried hydrogen bond network and associated changes in main chain dynamics for the stability of iso-1-cytochrome *c* and cooperative effects stemming from the introduction of His 26, we use a triple mutant cycle involving sequence positions 26, 52, and 67 (Figure 2). The triple mutant cycle can also be decomposed into six constituent double mutant cycles (*12*), allowing each pairwise interaction to be evaluated in two different contexts (opposite faces of the cube representing the triple mutant cycle in Figure 2). As a starting point for the triple mutant cycle, we use a variant we refer to as AcTM (*13*). We have chosen this variant as the starting point for the triple mutant cycle because the double mutant cycle that showed a strong cooperative interaction between introduction of His 26 and Ile 52 began with this variant (*6*). The AcTM variant has six mutations relative to WT iso-1-cytochrome *c* (T(-5)S, K(-2)L, H26N, H33N, H39Q, and C102S).

The pairwise energies of interaction for the double mutant cycles as well as the three way interaction energy for the

triple mutant cycle are used to evaluate the effect of the hydrogen bond network on the cooperativity of cytochrome *c* folding. We find that the strong cooperative interaction between His 26 and Ile 52 (*6*) is dissipated in the triple mutant variant. This observation is discussed in terms of changes in protein dynamics distant from a mutation site as mediated by changes in a hydrogen bond network.

MATERIALS AND METHODS

Site-Directed Mutagenesis. Site-directed mutagenesis was the method of choice for adding mutations to template DNA. All template DNA was the single stranded pRS/C7.8 yeast phagemid vector (*14*) except for the preparation of the AcH26F67 variant in which the single stranded template was the pRS425/CYC1 yeast phagemid vector containing the AcH26 variant (*13*). The mutations were added onto the iso-1-cytochrome *c* template using the unique restriction site elimination site-directed mutagenesis method (*15*) as previously described (*14*). All variants have a Cys 102 → Ser mutation to prevent formation of intermolecular disulfide bonds during physical studies. The presence of the desired mutations was confirmed using a Beckman CEQ8000 automated DNA sequencer. Preparation of yeast carrying phagemid with variant iso-1-cytochromes *c* was as described previously (*16*). Briefly, mutated double stranded phagemid DNA is transformed into the yeast GM-3C-2 strain of *S. cerevisiae,* which is cytochrome *c* deficient. Phenotypic screening was done to confirm the functionality of each variant. A curing procedure followed to confirm that each protein was being expressed from the pRS/C7.8 or pRS425/CYC1 phagemid DNA. The phagemid DNA was then reisolated from yeast and retransformed into bacterial cells for resequencing to ensure that no additional mutations occurred under the selective conditions used for cytochrome *c* expression and to further confirm the presence of the desired mutation.

Protein Isolation and Purification. Iso-1-cytochrome *c* variants were expressed and purified as described previously (*16*). Briefly, yeast YPG (1% yeast extract, 2% peptone, 3% glycerol) media was inoculated with cells containing the desired mutated gene in the phagemid DNA and grown to saturation in a New Brunswick BioFlo IIC fermentor. The cells were harvested and then lysed with a 2:1 mixture of 1 M NaCl and ethyl acetate. The lysate was treated with 50% ammonium sulfate to precipitate other proteins out of solution and then placed into 3500 molecular weight cutoff dialysis tubing and dialyzed against 12.5 mM sodium phosphate buffer, pH 7.2, 1 mM Na_2EDTA, 2 mM β-mercaptoethanol. The protein was further purified using CM Sepharose cation exchange chromatography and high-resolution cation exchange HPLC (BioRad UNO S6 column).

Protein Stability Determination. Protein denaturation experiments were carried out with the Applied Photophysics PiStar 180 circular dichroism spectrometer. Ellipticity at 222 nm was monitored with a baseline reference at 250 nm. A 20 mM Tris, 40 mM NaCl buffer at pH 7.0 was used. The temperature was kept constant at 25 °C using a circulating water bath (ThermoNESLAB RTE7). The protein concentration is ~4 μM. The 7 M gdnHCl was added to the protein sample using the Hamilton Microlab 500 series titrator. The unit is set up to take up a small volume of the protein sample from the sample cell holder and replace that volume with 7 M gdnHCl (in Tris/NaCl buffer) containing an equal concentration of the protein. The range of concentrations used depended on the stability of the variant.

The ellipticity as a function of [gdnHCl] is plotted using SigmaPlot 2000 (v. 7.01) and fit to eq 1 (*13*) using nonlinear least-squares methods. In this equation, the native (θ°_N) and denatured state ($\theta^\circ_D + m_D$[gdnHCl]) baselines and the unfolding region are fit simultaneously, assuming a linear dependence of the free energy on [gdnHCl]

$$\theta = \frac{(\theta^\circ_N) + \{(\theta^\circ_D + m_D[\mathrm{GdnHCl}])e^{(m[\mathrm{GdnHCl}]-\Delta G_u(H_2O)/RT)}\}}{1 + e^{(m[\mathrm{GdnHCl}]-\Delta G_u(H_2O)/RT)}} \quad (1)$$

represented by eq 2

$$\Delta G_u = \Delta G_u(H_2O) - m[\mathrm{gdnHCl}] \quad (2)$$

where $\Delta G_u(H_2O)$ is the free energy of unfolding extrapolated to zero denaturant concentration, and m is the rate of change of the free energy of unfolding, $\Delta G_{u,}$ as a function of denaturant concentration.

Determination of the Energy of Interaction. The energy of interaction is calculated by accounting for the stability contributions relative to the AcTM protein caused by single and double mutation in, respectively, double and triple mutant cycles. Eq 3 is used to calculate the energy of interaction for a double mutant cycle, while eqs 4 and 5 are used to calculate the energy of interaction for a triple mutant cycle (*10*, *11*). In eqs 3−5, the $\Delta\Delta G$ values are the difference in the stability between the single, double, and triple mutant variants and the AcTM (N26, N52, Y67) variant ($\Delta G_u(H_2O)_{variant} - \Delta G_u(H_2O)_{AcTM}$). Thus, for $\Delta^2 G_{int}$ and $\Delta^3 G_{int}$

$$\Delta^2 G_{int} = \Delta\Delta G_{double} - \Delta\Delta G_{single1} + \Delta\Delta G_{single2} \quad (3)$$

$$\Delta^3 G_{int} = \Delta^3 G_{int-1} - \sum \Delta^2 G_{int} \quad (4)$$

where

$$\Delta^3 G_{int-1} = \Delta\Delta G_{triple} - (\Delta\Delta G_{single1} + \Delta\Delta G_{single2} + \Delta\Delta G_{single3}) \quad (5)$$

a positive energy of interaction is indicative of a larger than additive effect (cooperative) for the mutations involved, whereas a negative energy of interaction indicates a less than additive interaction (anticooperative) for the mutations involved. Eq 3 is straightforward. If the sum of the stability changes in the single mutant variants equals the stability change for the double mutant variant, the effects of the two mutations are additive (i.e., $\Delta^2 G_{int} = 0$). If not, there is cooperativity or anticooperativity between the two mutations, depending on the sign of $\Delta^2 G_{int}$. For triple interaction energies, the situation is more complex. $\Delta^3 G_{int-1}$ determines if the effects on stability of the single mutations add up to the change in stability of the triple mutant variant relative to the protein without any of the mutations (AcTM in this case). Nonadditivity in $\Delta^3 G_{int-1}$ indicates the possibility that there may be a three way cooperative or anticooperative interaction between the three mutations. However, it is possible that

nonadditivity in Δ^3G_{int-1} is simply due to the effects of cooperativity or anticooperativity from the three possible pairwise interactions, Δ^2G_{int}, between the three mutation sites. In eq 4, these pairwise interactions are accounted for. If Δ^3G_{int-1} is nonadditive, but Δ^3G_{int} is zero, the nonadditivity in the triple mutant variant stability can be accounted for by the pairwise nonadditivities, Δ^2G_{int}, in the double variants. However, if Δ^3G_{int} is nonzero, there is a true three way cooperative or anticooperative interaction between the three mutations in the triple mutant variant.

Determination of the Error in the Energies of Interaction. The experimental error in $\Delta G_u(H_2O)$ is the standard deviation of three experiments unless otherwise indicated. In eqs 3−5, $\Delta G_u(H_2O)$ for the AcTM variant is subtracted from each term in the equation, as shown for the interaction energy of the double mutant cycle (eq 6).

$$\Delta^2G_{int} = (\Delta G_{double} - \Delta G_{AcTM}) - \{(\Delta G_{single1} - \Delta G_{AcTM}) + (\Delta G_{single2} - \Delta G_{AcTM})\} \quad (6)$$

Eq 6 simplifies to eq 7

$$\Delta^2G_{int} = \Delta G_{double} - \Delta G_{single1} - \Delta G_{single2} + \Delta G_{AcTM} \quad (7)$$

Thus, in calculating the experimental error, the multiple AcTM terms cancel out, and the square root of the sum of the squares of the error in the stability for each protein in the double mutant cycle gives the experimental error for Δ^2G_{int}.

$$\sigma_{\Delta^2G_{int}} = \sqrt{(\sigma_{\Delta G_{double}})^2 + (\sigma_{\Delta G_{single1}})^2 + (\sigma_{\Delta G_{single2}})^2 + (\sigma_{\Delta G_{AcTM}})^2} \quad (8)$$

Determination of the experimental errors for the triple mutant interaction energies, Δ^3G_{int} and Δ^3G_{int-1}, was done using eqs 9 and 10, respectively, as previously described by Stites and co-workers (*11*).

$$\sigma_{\Delta^3G_{int}} = \sqrt{\begin{array}{c}(\sigma_{\Delta G_{triple}})^2 + (\sigma_{\Delta G_{double1}})^2 + (\sigma_{\Delta G_{double2}})^2 + \\ (\sigma_{\Delta G_{double3}})^2 + (\sigma_{\Delta G_{single1}})^2 + (\sigma_{\Delta G_{single2}})^2 + \\ (\sigma_{\Delta G_{single3}})^2 + (\sigma_{\Delta G_{AcTM}})^2\end{array}} \quad (9)$$

$$\sigma_{\Delta^3G_{int-1}} = \sqrt{\begin{array}{c}(\sigma_{\Delta G_{triple}})^2 + (\sigma_{\Delta G_{single1}})^2 + (\sigma_{\Delta G_{single2}})^2 + \\ (\sigma_{\Delta G_{single3}})^2 + (2\sigma_{\Delta G_{AcTM}})^2\end{array}} \quad (10)$$

RESULTS

A triple mutant cycle was constructed and utilized to determine the energy of interaction between sequence positions 52 and 67, which participate in the buried hydrogen bond network, and position 26, which forms a hydrogen bond between the green and the N-yellow substructures in WT iso-1-cytochrome *c*. The triple mutant cycle comprises the AcTM variant, three single mutant variants (AcH26, AcI52, and AcF67), three double mutant variants (AcH26I52, AcH26F67, and AcI52F67), and a triple mutant (AcH26I52F67) as shown in Figure 2. The AcTM variant is the starting point in the triple mutant cycle. The triple mutant cycle also contains double mutant cycles allowing pairwise interactions between positions 26 and 52, 52 and 67, and 26 and 67 to be evaluated. The free energy of unfolding for each variant in the triple mutant cycle was determined using circular dichroism spectroscopy. The energy of interaction was determined for the double and triple cycles using eqs 3 and 4, respectively (Materials and Methods).

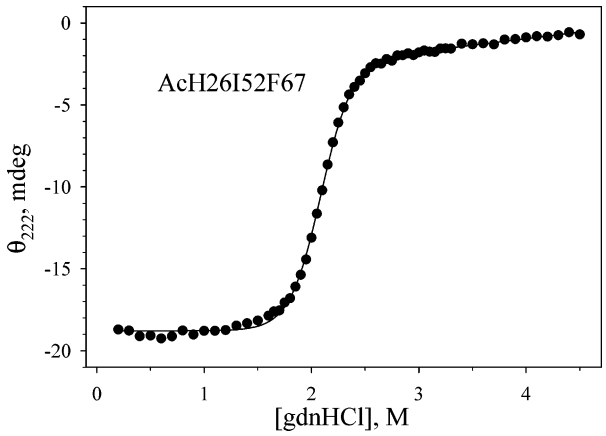

FIGURE 3: Denaturation curve for AcH26I52F67 iso-1-cytochrome *c* at pH 7.0 in 20 mM Tris, 40 mM NaCl, 25 °C. The ellipticity at 222 nm is plotted against [gdnHCl]. The continuous curve is a nonlinear least-squares fit to eq 1.

Previous work done in this laboratory (*6*), which used the N52I mutation as part of a set of double mutant cycles, showed that the Ile 52 mutation interacted strongly with the Asn 26 → His mutation. The triple mutant cycle studied here will determine whether the Tyr 67 → Phe mutation also interacts cooperatively with the His 26 mutation, how the Tyr 67→ Phe and Asn 52→ Ile mutations affect each other, and how all three mutations interact. Hammack et al. (*17*) have previously determined that the N-terminal amino group of the protein competes with histidine for binding to the sixth coordination site of the heme under denaturing conditions. The variants used in this study all have an acetylated N-terminal amino group (affected by T(-5)S and K(-2)L mutations; see ref *13*) to prevent the N-terminal amino group from binding to the heme in the denatured state. Other side chain binding to the heme in the denatured state (*13*) is eliminated in the AcTM variant since His 33 and 39, present in WT iso-1-cytochrome *c*, have been converted to Asn and Gln, respectively. Removal of these denatured state interactions limits complexities in the denatured state, which could complicate analysis of the triple mutant cycle.

Guanidine Hydrochloride Denaturation Data. A typical gdnHCl denaturation curve is shown in Figure 3. The thermodynamic parameters derived from gdnHCl denaturation data are presented in Table 1. The $\Delta G_u(H_2O)$ energies of unfolding range from 3.93 to 9.37 kcal/mol. The most stable variant is the AcH26I52 double mutant. The triple mutant variant is the second most stable protein; it is only slightly and within a margin of error less stable than the AcH26I52 variant but is much more stable than the other two double mutant variants. The single sequence mutation variants are 0.8−2.7 kcal/mol more stable than the AcTM protein, with the AcI52 variant being the most stable protein among them.

Table 1: Free Energies of Unfolding for Variants of the Triple Mutant Cycle[a]

variant	$\Delta G(H_2O)$ (kcal/mol)	m (kcal/(mol × M))[b]	$C_{1/2}$ (M)[c]
AcTM[d]	3.93 ± 0.15	3.71 ± 0.18	1.06 ± 0.04
AcF67	5.61 ± 0.15	4.28 ± 0.08	1.31 ± 0.01
AcH26[d]	4.71 ± 0.16	4.63 ± 0.15	1.02 ± 0.03
AcI52[e]	6.63 ± 0.23	3.82 ± 0.19	1.74 ± 0.06
AcH26F67	5.86 ± 0.20	4.77 ± 0.20	1.23 ± 0.04
AcI52F67	7.69 ± 0.26	3.88 ± 0.01	1.98 ± 0.07
AcH26I52[e]	9.37 ± 0.24	4.99 ± 0.15	1.88 ± 0.05
AcH26I52F67	8.98 ± 0.44	4.25 ± 0.18	2.11 ± 0.04

[a] All data collected at pH 7 and 25 °C in 20 mM Tris, 40 mM NaCl buffer. The data presented are the average of three trials for all variants except for AcH26I52F67; five trials were done with this variant. All reported errors are standard deviations. [b] The m value is the change in free energy with respect to the change in [gdnHCl]. [c] $C_{1/2}$ value represents the [gdnHCl] at which half of the protein is denatured. [d] The data for AcTM and AcH26 variants are from Hammack et al. (*13*). [e] Data for the AcI52 and AcH26I52 variants are from ref *6*.

Table 2: Pairwise Interaction Energies

variant[a] or residues interacting[b]	$\Delta\Delta G_{double}$[c]	$\Sigma\Delta\Delta G_{single}$	Δ^2G_{int}[d]	$^2m_{int}$[e]
AcH26F67	1.93	2.46	−0.5 ± 0.3	−0.4 ± 0.2
H26/F67 (AcI52)	2.35	3.80	−1.5 ± 0.6	−0.8 ± 0.3
AcI52F67	3.76	4.38	−0.6 ± 0.4	−0.5 ± 0.3
I52/F67 (AcH26)	4.27	5.81	−1.5 ± 0.4	−0.9 ± 0.3
AcH26I52[f]	5.44	3.48	2.0 ± 0.4	0.3 ± 0.3
H26/I52 (AcF67)	3.37	2.33	1.0 ± 0.6	−0.1 ± 0.3

[a] Where a variant is listed, the double mutant cycle starts with the AcTM variant. [b] Where two residues are listed, the starting variant is indicated in brackets. [c] $\Delta\Delta G_{double} = \Delta G_{double} - \Delta G_{AcTM}$. For interacting residues, the last term in the equation is the ΔG for the variant in brackets and ΔG_{triple} substitutes for ΔG_{double}. [c] $\Sigma\Delta\Delta G_{single} = (\Delta G_{single\ 1} - \Delta G_{AcTM}) + (\Delta G_{single\ 2} - \Delta G_{AcTM})$. For interacting residues, the ΔG for the variant in brackets is used in place of ΔG_{AcTM}. [d] $\Delta^2G_{int} = \Delta\Delta G_{double} - \Sigma\Delta\Delta G_{single}$. [e] $^2m_{int} = \Delta m_{double} - \Sigma\Delta m_{single}$. [f] Data taken from Wandschneider et al. (*6*).

Some variation in m values is observed. The m values, which represent the change in free energy with respect to the change in [gdnHCl], range from 3.71 kcal/(mol × M) for the AcTM variant to 4.99 kcal/(mol × M) for AcH26I52. In general, the m value is larger (4.3−5.0 kcal/(mol × M)) for variants containing a histidine at position 26. The midpoint denaturant concentrations for unfolding, $C_{1/2}$, range from 1.02 to 2.11 M gdnHCl, with the AcH26I52F67 variant having the highest $C_{1/2}$.

Additivity of Stability. The energy of interaction for the double mutant cycles was determined and is presented in Table 2. A positive value for the energy of interaction indicates that the two mutations reinforce one another, while a negative value signifies that the two mutations interfere with each other. The six double mutant cycles allow evaluation of an interaction energy, Δ^2G_{int}, for each of the three pairs of positional mutations in two different contexts. For the interaction of the His 26 and Ile 52 mutations, Δ^2G_{int} is always positive. In the presence of Phe 67, Δ^2G_{int} is about half as large as previously seen in the presence of Tyr 67 (*6*). For the interaction between the Ile 52 and the Phe 67 mutations, Δ^2G_{int} is always negative. The magnitude of Δ^2G_{int} for this interaction is much larger in the His 26 background than in the Asn 26 background. In previous work using thermal denaturation methods (*5*), the stability effects of the N52I and Y67F mutations were additive in the wild type (His 26, C102T) background. The difference in pH (4.7 vs 7.0 here) and the temperature (53.6 vs 25 °C here) at which the stability differences were reported in the previous experiments may account for the observed differences. Finally, for the interaction between the His 26 and the Phe 67 mutations, Δ^2G_{int} is always negative. The magnitude of the interaction energy is much larger in the Ile 52 background than in the Asn 52 background.

Since the m values vary, it is also useful to assess whether these changes are additive or not (*18*). In Table 2, pairwise nonadditivities in m values, $^2m_{int}$, are calculated. For the interaction between His 26 and Ile 52, the m values in the double mutant cycle are additive within error ($^2m_{int} \approx 0$). For the other pairs of interactions, $^2m_{int}$ is negative.

For the triple mutant variant, AcH26I52F67, Δ^3G_{int-1} is −0.1 ± 0.6, indicating that the stability effects of the individual mutations are additive in the triple mutant variant, as discussed in the Materials and Methods. The apparent additivity requires that the strong positive interaction energy of His 26 and Ile 52 be canceled out, presumably by the slightly negative interaction energy of His 26 with Phe 67 and of Phe 67 with Ile 52. However, the triple mutant additivity also requires a slightly negative triple interaction energy, Δ^3G_{int}, of −0.9 ± 0.7 kcal/mol. The negative value of Δ^3G_{int} indicates that there is a net three-way unfavorable interaction between His 26, Phe 67, and Ile 52 that is not accounted for by the pairwise interactions between the three sequence position mutations (see Materials and Methods). Thus, the underlying basis of the observed additivity of the stability effects of the single mutations when combined in the triple mutant variant is complex.

Nonadditivities also exist in the m values of the triple mutant variant relative to the single mutant variants. In analogy to Δ^3G_{int-1} (eq 5), we calculate $^3m_{int-1}$ to be −1.1 ± 0.5 kcal/(mol × M), indicating substantial nonadditivity in the m value of AcH26I52F67 relative to the single mutant variants. When the pairwise nonadditivities in m values are accounted for, we find that the three way nonadditive interaction in the m values, $^3m_{int}$ (calculated as for Δ^3G_{int}, eq 4 in Materials and Methods), is −0.4 ± 0.4 kcal/(mol M). So, within error, much of the nonadditivity in the m value of AcH26I52F67 is accounted for by the pairwise nonadditivities in the m value.

DISCUSSION

General Observations on Δ^2G_{int} and Δ^3G_{int} Values. A key observation in this work is that the strong cooperative interaction energy (2.0 ± 0.4 kcal/mol) observed in the N52I/N26H double mutant variant is dissipated in the triple mutant variant, AcH26I52F67, such that the overall stability appears to be simply additive based on the effects of the individual single mutations. As can be seen in Table 2, only the interaction between the His 26 and Ile 52 mutations leads to a positive or cooperative energy of interaction (Δ^2G_{int}). The other double and triple interaction energies (Δ^2G_{int} and Δ^3G_{int}) are negative or anticooperative. Previous work has indicated that nonadditive stability effects primarily result from mutations at adjacent sites in proteins (*10*, *11*, *19*−*21*). However, for staphylococcal nuclease, a large number of nonadditive double mutant cycles were observed, and in

many cases, the mutation sites were distant in the native structure (*18*). Large nonadditivities in *m* values were observed in this case, which correlated with nonadditivities in Δ^2G_{int}, leading to the conclusion that the denatured state played a significant role in the observed Δ^2G_{int} values. While positions 52 and 67 are adjacent to each other in the structure of iso-1-cytochrome *c*, position 26 is distant from both positions 52 and 67 (Figure 1). Clearly, nonadditivity exists both between the mutations at positions 26 and 52 and the mutations at positions 26 and 67. Here, we analyze the interaction energies, Δ^2G_{int} and Δ^3G_{int}, in the context of the available X-ray structure data and find that a prime factor in nonadditive effects on stability is the bridging hydrogen bond between the ring nitrogens of the His 26 side chain and the carbonyl of Glu 44 and the amide NH of Asn 31 (Figure 1). On the basis of crystallographic thermal factors, the strength of the His 26/Glu 44 intersubstructure hydrogen bond appears to be modulated by changes in segmental dynamics caused by modifications to the buried hydrogen bond network, leading to cooperative or anticooperative effects in stability that operate over long distances. We also discuss the possible role of the denatured state in the observed nonadditivity.

Possible Effects of Mutations in the AcTM Variant Relative to WT iso-1-Cytochrome c. In the analysis that follows, we use X-ray structures of iso-1-cytochrome *c* that have the Y67F, N52I, or both of these mutations in the C102T pseudo-WT background. The starting point for the triple mutant cycle used here is the AcTM variant, which has six mutations (T(-5)S, K(-2)L, H26N, H33N, H39Q, and C102S) relative to the C102T pseudo-WT, as noted in the introductory paragraphs. So, some discussion of the potential impact of these mutations on the AcTM variant relative to WT (C102T) iso-1-cytochrome *c* is warranted. The first two mutations, T(-5)S, K(-2)L, are located in the disordered N-terminal extension (*8*) of iso-1-cytchrome *c* and cause the protein to be acetylated in vivo (*13*). The stability of the AcTM and TM (H26N, H33N, H39Q, and C102S) variants are identical so the effects of these mutations, and the resulting N-terminal acetylation, are minimal (*13*), as expected, given the disordered nature of the structure of iso-1-cytochrome *c* in this region. Positions 33 and 39 are at solvent exposed sites in iso-1-cytochrome *c* (*8*). Solvent exposed sites typically have minimal impact on the stability of proteins (*22*). In the case of positions 33 and 39, the pK_a values of the histidine side chains are near 6.8 (*23*), close to the value expected for an isolated histidine. Thus, there is no evidence for either of these residues participating in strong electrostatic interactions that could strongly affect the native structure of the protein. In fact, introduction of the N33H mutation into AcTM to produce the AcH33 variant produces no change in the stability of the protein (*13*). Adding the Q39H mutation to AcTM to produce AcH39 does decrease stability by ~0.8 kcal/mol (*13*). However, when this mutation is added to the TM variant, there is no change in stability (*24*). Thus, these solvent exposed residues appear to minimally affect the stability of iso-1-cytochrome *c*. The final difference between the AcTM variant and the proteins used in X-ray structure analysis of the N52I and Y67F mutations is the presence of the C102T mutation versus the C102S mutation used here. These two mutations are standard in thermodynamic studies on iso-1-cytochrome *c*, as they prevent intermolecular disulfide bond formation. Careful thermodynamic studies on the C102S and C102T pseudo-WT iso-1-cytochromes *c* show that the C102S variant is 0.6 kcal/mol less stable at pH 7.5 and 1.4 kcal/mol less stable at pH 4.5 (*24*−*27*). Since position 102 is partially buried, the additional methyl group would be expected to enhance stability of the C102T variant relative to the C102S variant. So, we cannot rule out the possibility that this difference could affect local dynamics. The measured gdnHCl *m* values and the ΔC_p values for the two pseudo-WT proteins are within error the same, indicating that these changes at position 102 do not affect the change in solvent-exposed surface associated with unfolding of the protein. This observation argues against the C102T to C102S change having a substantial effect on the packing of the core of the protein where the buried hydrogen bond network is located. The NMR structure of oxidized iso-1-cytochrome *c* was done with the C102S pseudo-WT (*28*), and the X-ray structure of oxidized iso-1-cytochrome *c* was done with the C102T pseudo-WT (*8*). The structures are very similar (average backbone rmsd of 0.88 Å), so the stability difference caused by the C102S versus the C102T mutation does not appear to translate into structural differences. Except for positions 102 and 26 (which is part of our thermodynamic cycle), all of the mutations in the AcTM variant are at the periphery of the protein and minimally affect the thermodynamic properties of iso-1-cytochrome *c*. Thus, we believe it is unlikely that they strongly perturb the buried hydrogen bond network of iso-1-cytochrome *c* as seen in the X-ray structures of the C102T pseudo-WT iso-1-cytochrome *c* (*8*) and the N52I, Y67F, and N52I/Y67F variants (*7*, *9*). The strong stabilizing effect of the N52I and Y67F mutations in the AcTM background, as observed in the C102T pseudo-WT background (*4*, *5*), suggests that similar effects are occurring in the core of the protein in both cases.

Positive Interaction between His 26 and Ile 52. As reported previously by Wandschneider et al. (*6*), the energy of interaction between these two mutation sites is strongly positive in the Tyr 67 background. Here, we find that this positive interaction, although smaller, is maintained in the Phe 67 background. Wandschneider et al. (*6*) offered reasons for this very favorable interaction between these two residues. Briefly, His 26 is a highly conserved residue that forms a bridging hydrogen bond between Glu 44 and Asn 31 (Figure 1) and is believed to be important for the structure and function of the protein (*29*); it is found in the green substructure of the protein. Position 52, when mutated from an Asn to an Ile, is a stabilizing mutation within the protein and is found in the least stable N-yellow substructure of the protein as reported by Englander and co-workers (*1*, *2*). An important reason for the cooperative interaction relates to the strengthening of the His 26/Glu 44 hydrogen bond (Table 3), which appears to be caused by the decrease in main chain dynamics of the N-yellow substructure as evidenced by crystallographic thermal factors (Figure 4; compare WT and N52I thermal factors for residues 40−57). The lower magnitude of Δ^2G_{int} in the Phe 67 background can be attributed to the effects of this mutation on the His 26/Glu 44 hydrogen bond, which appears to be linked to an increase in dynamics of the main chain near Glu 44 (Figure 4 and Table 3). Relative to the presence of only Ile 52, when both Phe 67 and Ile 52 are present, the His 26 to Glu 44 hydrogen bond is longer, and the dynamics of the main chain at Glu 44 is increased. Thus, the cooperative interaction of the Ile

Table 3: Thermal Factor and Hydrogen Bond Length Data[a]

variant	thermal factor (Å^2) main chain Glu 44	hydrogen bond length (Å) Glu 44(CO)−His 26 side chain	thermal factor (Å^2) main chain Asn 31	hydrogen bond length (Å) Asn 31(NH)−His 26 side chain
N52I	13.1	2.73	11.9	2.77
WT	13.5	3.10	2.0	2.73
Y67F/N52I	17.1	2.97	10.4	2.57
Y67F	25.8	3.60	10.8	2.77

[a] Data from Protein Data Bank (*30*) 2YCC (oxidized wild type), 1CTY (oxidized Y67F variant), 1CRG (oxidized N52I variant), and 1CRI (oxidized N52I/Y67F variant).

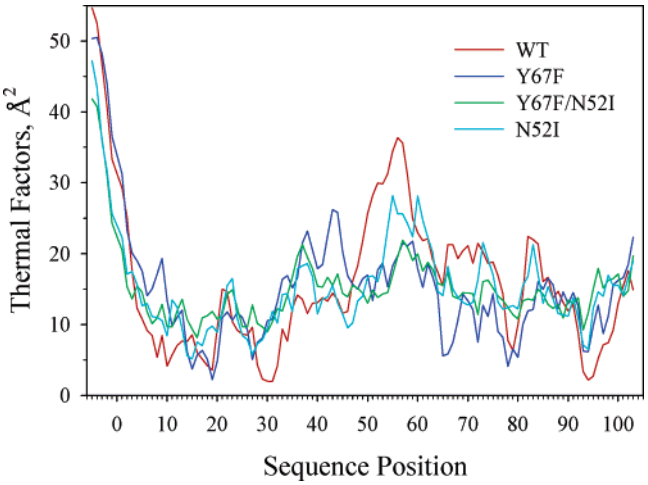

FIGURE 4: Main chain thermal factors vs sequence position for the WT (red), Y67F (blue), Y67F/N52I (green), and N52I (cyano) iso-1-ferricytochromes *c*. The thermal factors are normalized to the average thermal factor of the WT oxidized protein structure to account for overall differences in the thermal factors of the individual structures (*7*). Data are taken from the Protein Data Bank (*30*) 2YCC (WT), 1CTY (Y67F), 1CRG (N52I), and 1CRI (N52I/Y67F).

52 and His 26 mutations is dampened due to less stabilization of the His 26 to Glu 44 hydrogen bond in the Phe 67 context. It is important to note that crystallographic thermal factors do not correlate exactly with solution measurements of protein dynamics, such as NMR monitored hydrogen exchange (*31*), when these values are compared for individual residue positions. However, for iso-1-cytochrome *c* (*31*), in general the lowest thermal factors in the X-ray structural data correspond to the regions of the protein (blue substructure, N- and C-terminal helices) most protected from hydrogen exchange, and the highest thermal factors correspond to the area least protected from hydrogen exchange, the least stable, N-yellow substructure. However, because of this ambiguity, our analysis, in general, will focus initially on gain or loss of hydrogen bonding and secondarily on the changes in crystallographic thermal factors that act to alter hydrogen bonding, particularly between His 26 and Glu 44.

It is possible that the hydrogen bond between His 26 and Asn 31 could play a role in the nonadditive stability effects, as well. Relative to the pseudo-WT (C102T) structure, the main chain dynamics of Asn 31 is increased but similar in all variants (Table 3). The variation in the His 26/Asn 31 (main chain amide NH) hydrogen bond length is also small as compared to the His 26/Glu 44 (main chain carbonyl) hydrogen bond length in the pseudo-WT (C102T) and variant structures (see Table 3). So, it appears that the hydrogen bond between His 26 and Asn 31 likely plays a smaller role in the observed nonadditivities in Δ^2G_{int}.

Negative Interaction between His 26 and Phe 67. As noted previously, His 26 is a highly conserved residue in cytochrome *c*. The residue is a part of a hydrogen bond network involving Asn 31 and Glu 44 and is a stabilizing factor in the protein (*29*). His 26 and Tyr 67 interact anticooperatively, producing a negative Δ^2G_{int} in both the Asn 52 and the Ile 52 contexts. The anticooperativity is more significant in the Ile 52 context.

The mutation of Tyr 67 to Phe causes a substantial increase in the Glu 44/His 26 hydrogen bond length (Table 3), leading to an anticooperative interaction, Δ^2G_{int}, between the His 26 and Phe 67 mutations. Particularly relevant to the anticooperative interaction between His 26 and Phe 67 is the increase in main chain dynamics between residues 35 and 45 (see Figure 4 and Table 3) as reported by Berghuis and coworkers (*9*). Much of the increased mobility in this region appears to result from maintenance of the Asn 52 side chain to heme propionate A hydrogen bond in the oxidized state when the Y67F mutation is present, a hydrogen bond that is broken when the WT protein is oxidized. The collateral effect of retention of this hydrogen bond appears to be breakage of the hydrogen bonds between heme propionate A and water 168 and between water 121 and the Arg 38 side chain, which are present in WT oxidized cytochrome *c*. Loss of these hydrogen bonds leads to increased dynamics between residues 35 and 45 (*9*). The increased mobility of Glu 44 likely weakens the Glu 44/His 26 hydrogen bond, as indicated by the increased hydrogen bond length (see Table 3). In the Ile 52 context, Δ^2G_{int} becomes 1 kcal/mol more negative paralleling the 1 kcal/mol decrease in cooperative stabilization between His 26 and Ile 52 in the Phe 67 versus the Tyr 67 context. In both cases, the increased His 26/Glu 44 hydrogen bond length in the Y67F/N52I versus the N52I iso-1-cytochromes *c* is likely responsible for the context dependent changes in Δ^2G_{int}.

Negative Interaction between Ile 52 and Phe 67. As discussed in the introductory paragraphs, significant changes in the buried hydrogen bond network occur with the mutations at these two residues, a hydrogen bond network involving Met 80, Thr 78, Tyr 67, and Asn 52 (*7*−*9*). The N52I mutation brings about the displacement of the Wat 166 molecule, which appears to be a stabilizing factor in that variant (*7*). The Y67F mutation, however, is not accompanied by a displacement of the Wat 166 molecule. Moreover, an additional water molecule, Wat 300, is introduced into the hydrogen bond network. The N52I−Y67F mutation displaces all internal water molecules and forms an internal cavity of only 8 Å^3, leaving only the heme pyrrole D propionate to Thr 78 side chain hydrogen bond.

The interaction energy between Phe 67 and Ile 52 is negative in both the Asn 26 and the His 26 contexts being more significant in the presence of His 26. Examination of

the effects of changes in the hydrogen bond network of single mutation variants versus the double mutation variant on the main chain dynamics of cytochrome *c* yields a possible explanation for the negative energy of interaction. An important factor in the increased stability of the Y67F variant is the Asn 52 to heme propionate A hydrogen bond in the oxidized protein. This hydrogen bond is removed when both the Ile 52 and the Phe 67 mutations are present. The strong impact of this hydrogen bond on the dynamics of the C-terminal half of the protein is apparent in Figure 4 (compare data for the Y67F variant to the WT data). In general, the dynamics of the Y67F/N52I protein is intermediate to that of the N52I and Y67F variants (Figure 4). Thus, combined the two mutations likely weaken van der Waals interactions operative in optimally stabilizing each of the single mutants. The net effect is a slightly negative nonadditivity. The amplification of the negative Δ^2G_{int} in the His 26 context again relates to the effects of the Ile 52 mutation versus the Ile 52/Phe 67 double mutation on the intersubstructure hydrogen bond between the His 26 side chain and the Glu 44 main chain carbonyl (Table 3).

Negative Interaction in the Triple Mutant Variant. The energy of interaction, Δ^3G_{int}, for the triple mutant variant was calculated to be -0.9 ± 0.7 kcal/mol. Although the cumulative error in Δ^3G_{int} is large, the magnitude of Δ^3G_{int} is similar to the decrease in Δ^2G_{int} for the interaction between His 26 and Ile 52 in the presence of Phe 67. Thus, the Δ^3G_{int} can be viewed as a weakening of the strong His 26 side chain to Glu 44 main hydrogen bond when only Ile 52 is present by the addition of Phe 67 (see Figure 4 and Table 3). The small combined interferences from negative Δ^2G_{int} for the two double mutant variants (F67/I52 and F67/H26) and the negative Δ^3G_{int} for the triple mutant variant act to dissipate the highly favorable Δ^2G_{int} for the N26H and N52I mutations. The interesting result is that these nonadditivities arise from incompatible changes in a hydrogen bond network that change the dynamics of the protein at sites distant from the site of mutation. These incompatibilities clearly modulate not only the strength of the His 26/Glu 44 hydrogen bond but also lead to changes in dynamics throughout the protein, which likely affect the van der Waals stabilization (packing) of the protein. The net effect is a triple mutant variant with apparent additive stability relative to the single mutant variants (Δ^3G_{int-1}).

Denatured State Effects on the Triple Mutant Cycle. In any mutational thermodynamic cycle where a mutation can affect either of two states of a macromolecule, care must always be taken in attributing the observed effects to one state or the other (*32*). In the previous discussion, we have interpreted the data in terms of effects on native state stability based on available crystallographic data. In work on staphylococcal nuclease (*18*), significant nonadditivity was observed for denaturant *m* values, as was a significant correlation between Δ^2G_{int} and $^2m_{int}$. We observe the same nonadditivity in *m* values here, as well as a significant correlation between Δ^2G_{int} and $^2m_{int}$ ($r^2 = 0.988$). The slope of this correlation is 3.22 M, somewhat larger than the slope of the Δ^2G_{int} versus $^2m_{int}$ correlations observed with staphylococcal nuclease. So, it is possible that the nonadditivities we observe in the free energy of unfolding in the triple mutant cycle involving positions 26, 52, and 67 have contributions from the denatured state. In previous work from this laboratory, involving a set of double mutant cycles that used the N52I mutation in combination with introduction of histidines at various sequence positions (*6*), we noted that the presence or absence of the N52I mutation has no impact on the thermodynamics of loop formation in the gdnHCl denatured state for a wide range of loop sizes (*33*). Thus, for gdnHCl denaturation, the effect of the N52I mutation on the denatured state appears to be small. For the N26H mutation, the primary effect on the denatured state is the introduction of a closed His 26-heme loop in the denatured state. In the calculation of Δ^2G_{int} for double mutant cycles involving His 26, the His 26−heme loop is present in the denatured state of the double mutant variant and one of the single mutant variants. Therefore, its thermodynamic effect is subtracted out in the calculation of Δ^2G_{int} (see eqs 3 and 7, Materials and Methods). The same is true for the calculation of Δ^3G_{int-1}, the triple mutant variant and only one of the single mutant variants will have the His 26−heme loop in the denatured state, so its effect will again be subtracted out (see eq 5, Materials and Methods). Since neither Δ^3G_{int-1} nor any of the Δ^2G_{int} values are affected by the His 26−heme loop, the calculation of Δ^3G_{int} should be free of denatured state contributions from His 26−heme loop formation (eq 4, Materials and Methods). In the case of the Y67F mutation, we do not have thermodynamic evidence as we do for the N52I mutation, indicating that its affect on denatured state thermodynamics is small. So, we cannot completely rule out the possibility of a denatured state contribution this case. Although due to the similarity in the Tyr and Phe side chains, it is likely that the effect on the denatured state is small.

We have nonadditive *m* values in the triple mutant cycle and its constituent double mutant cycles, which have been interpreted in terms of nonadditive thermodynamic effects operating in the denatured state. Yet, we have denatured state loop formation data, which indicate that the N52I mutation has at most a minor effect on the denatured state of iso-1-cytochrome *c*. The question is how to reconcile these two observations. It is interesting to note, for the single mutant variants, that the Ile 52 mutation (AcI52) has only a minor effect on the *m* value relative to the AcTM variant. The single mutant variants, AcH26 and AcF67, lead to increases in the *m* value of approximately 0.9 and 0.6 kcal/(mol M), respectively. In both cases, X-ray structural data indicate that new hydrogen bonds are made in the native state. For introduction of His 26, a substructure bridging hydrogen bond is made, and for introduction of Phe 67, a new hydrogen bond between Asn 52 and heme propionate A is made, which strongly decreases the dynamics in the C-terminal half of the protein. In the presence of these hydrogen bonds, it is likely that the native states are less flexible, which might on average increase the buried hydrophobic surface of the native state leading to the observed increases in *m* values. It is also possible that the presence of these hydrogen bonds make unfolding more cooperative, leading to a more abrupt transition and a larger *m* value. Since our loop formation data do not support a denatured state explanation for nonadditivities in *m* values, we tentatively suggest that the nonadditivities in the *m* values may relate to changes in native state hydrogen bonding. The behavior of the nonadditivities in $^2m_{int}$ is qualitatively consistent with this proposal. For example, in the case of the AcI52F67 variant, $^2m_{int}$ is

negative, and due to the added N52I mutation, the Asn 52 to heme propionate hydrogen bond in the AcF67 variant can no longer be made.

Summary. In conclusion, we have constructed a triple mutant cycle and investigated the energy of interaction among the residues in the double mutant variants and the triple mutant variant of the cycle involving three known stabilizing residues in iso-1-ferricytochrome *c*. Within this set of variants, only the N52I and N26H mutations show a strong positive cooperative interaction, as observed previously (*6*). All other pairwise interactions are negative (anticooperative). In combination with existing crystallographic results, the data indicate that the intersubstructure hydrogen bond between His 26 and Glu 44 is an important contributor to cooperative interactions in cytochrome *c* at the level of tertiary structure. The buried hydrogen bond network, associated with the residues at positions 52 and 67, appears to play an important role in modulating the strength of the Glu 44/His 26 intersubstructure hydrogen bond. Changes in the buried hydrogen bond network produce widely distributed changes in backbone dynamics, providing a mechanism for both positive and negative nonadditivity between distant mutation sites.

REFERENCES

1. Bai, Y., Sosnick, T. R., Mayne, L., and Englander, S. W. (1995) Protein folding intermediates: Native-state hydrogen exchange, *Science 269*, 192−197.
2. Krishna, M. M. G., Lin, Y., Rumbley, J. N., and Englander, S. W. (2003) Cooperative omega loops in cytochrome *c*: Role in folding and function, *J. Mol. Biol. 331*, 29−36.
3. Hickey, D. R., Berghuis, A. M., Lafond, G., Jaeger, J. A., Cardillo, T. S., McLendon, D., Das, G., Sherman, F., Brayer, G. D., and McLendon, G. (1991) Enhanced thermodynamic stabilities of yeast iso-1-cytochromes *c* with amino acid replacements at positions 52 and 102, *J. Biol. Chem. 266*, 11686−11694.
4. Linske-O'Connell, L. I., Sherman, F., and McLendon, G. (1995) Stabilizing amino acid replacements at position 52 in yeast iso-1-cytochromes *c*: In vivo and in vitro effects, *Biochemistry 34*, 7094−7102.
5. Lett, C. M., Berghuis, A. M., Frey, H. E., Lepock, J. R., and Guillemette, J. G. (1996) The role of a conserved water molecule in the redox-dependent thermal stability of iso-1-cytochrome *c*, *J. Biol. Chem. 271*, 29088−29093.
6. Wandschneider, E., Hammack, B. N., and Bowler, B. E. (2003) Evaluation of cooperative interactions between substructures of iso-1-cytochrome *c* using double mutant cycles, *Biochemistry 42*, 10659−10666.
7. Berghuis, A. M., Guillemette, J. G., McLendon, G., Sherman, F., Smith, M., and Brayer, G. D. (1994) The role of a conserved internal water molecule and its associated hydrogen bond network in cytochrome *c*, *J. Mol. Biol. 236*, 786−799.
8. Berghuis, A. M., and Brayer, G. D. (1992) Oxidation state-dependent conformational changes in cytochrome *c*, *J. Mol. Biol. 223*, 959−976.
9. Berghuis, A. M., Guillemette, J. G., Smith, M., and Brayer, G. D. (1994) Mutation of tyrosine-67 to phenylalanine in cytochrome *c* significantly alters the local heme environment, *J. Mol. Biol. 235*, 1326−1341.
10. Chen, J., and Stites, W. E. (2001) Energetics of side chain packing in staphylococcal nuclease assessed by systematic double mutant cycles, *Biochemistry 40*, 14004−14011.
11. Chen, J., and Stites, W. E. (2001) Higher-order packing interactions in triple and quadruple mutants of staphylococcal nuclease, *Biochemistry 40*, 14012−14019.
12. Horovitz, A., and Fersht, A. R. (1992) Cooperative interactions during protein folding, *J. Mol. Biol. 224*, 733−740.
13. Hammack, B. N., Smith, C. R., and Bowler, B. E. (2001) Denatured state thermodynamics: residual structure, chain stiffness, and scaling factors, *J. Mol. Biol. 311*, 1091−1104.
14. Smith, C. R., Mateljevic, N., and Bowler, B. E. (2002) Effects of topology and excluded volume on protein denatured state conformational properties, *Biochemistry 41*, 10173−10181.
15. Deng, W. P. D., and Nickoloff, J. A. (1992) Site-directed mutagenesis on virtually any plasmid by eliminating a unique restriction site, *Anal. Biochem. 200*, 81−88.
16. Herrmann, L., Flatt, P., and Bowler, B. E. (1996) Site-directed replacement of the invariant lysine 73 of *Saccharomyces cerevisiae* iso-1-cytochrome *c* with all ribosomally encoded amino acids, *Inorg. Chim. Acta 242*, 97−103.
17. Hammack, B., Godbole, S., and Bowler, B. E. (1998) Cytochrome *c* folding traps are not due solely to histidine−heme ligation: Direct demonstration of a role for N-terminal amino group−heme ligation, *J. Mol. Biol. 275*, 719−724.
18. Green, S. M., and Shortle, D. (1993) Patterns of nonadditivity between pairs of stability mutations in Staphylococcal nuclease, *Biochemistry 32*, 10131−10139.
19. Aldrich, R. W., and Fodor, A. A. (2004) On evolutionary conservation of thermodynamic coupling in proteins, *J. Biol. Chem. 279*, 19046−19050.
20. Jain, R. K., and Ranganathan, R. (2004) Local complexity of amino acid interactions in a protein core, *Proc. Natl. Acad. Sci. U.S.A. 101*, 111−116.
21. Skinner, M. M., and Terwilliger, T. C. (1996) Potential use of additivity of mutational effects in simplifying protein engineering, *Proc. Natl. Acad. Sci. U.S.A. 93*, 10753−10757.
22. Alber, T., Dao-pin, S., Nye, J. A., Muchmore, D. C., and Matthews, B. W. (1987) Temperature-sensitive mutations of bacteriophage T4 lysozyme occur at sites with low mobility and low solvent accessibility in the folded protein, *Biochemistry 26*, 3754−3758.
23. Robinson, M. N., Boswell, A. P., Huang, Z. X., Eley, C. G. S., and Moore, G. R. (1983) The conformation of eukaryotic cytochrome *c* around residues 39, 57, 59, and 74, *Biochem. J. 213*, 687−700.
24. Godbole, S., Hammack. B., and Bowler, B. E. (2000) Measuring denatured state energetics: Deviations from random coil behavior and implications for the folding of iso-1-cytochrome *c*, *J. Mol. Biol. 296*, 217−228.
25. Herrmann, L. M., and Bowler, B. E. (1997) Thermal denaturation of iso-1-cytochrome *c* variants: Comparison with solvent denaturation, *Protein Sci. 6*, 657−665.
26. Cohen, D. S., and Pielak, G. J. (1994) Stability of yeast iso-1-cytochrome *c* as a function of pH and temperature, *Protein Sci. 3*, 1253−1260.
27. Betz, S. F., and Pielak, G. J. (1992) Introduction of a disulfide bond in cytochrome *c* stabilizes a compact denatured state, *Biochemistry 31*, 12337−12344.
28. Banci, L., Bertini, I., Bren, K. L., Gray, H. B., Sompornpisut, P., and Turano, P. (1997) Solution structure of oxidized *Saccharomyces cerevisiae* iso-1-cytochrome *c*, *Biochemistry 36*, 8992−9001.
29. Fetrow, J. S., Dreher, U., Wiland, D. J., Schaak, D. L., and Boose, T. L. (1998) Mutagenesis of histidine 26 demonstrates the importance of loop−loop and loop−protein interactions for the function of iso-1-cytochrome *c*, *Protein Sci. 7*, 994−1005.
30. Berman, H. M., Westbrook, J., Feng, Z., Gilliland, G., Bhat, T. N., Weissig, H., Shindyalov, I. N., and Bourne, P. E. (2000) The protein data bank, *Nuc. Acids Res. 28*, 235−242.
31. Baxter, S. M., and Fetrow, J. S. (1999) Hydrogen exchange behavior of [U-^{15}N]-labeled oxidized and reduced iso-1-cytochrome *c*, *Biochemistry 38*, 4493−4503.
32. Di Cera, E. (1998) Site-specific analysis of mutational effects in proteins, *Adv. Protein Chem. 51*, 59−119.
33. Wandschneider, E., and Bowler, B. E. (2004) Conformational properties of the iso-1-cytochrome *c* denatured state: Dependence on guanidine hydrochloride concentration, *J. Mol. Biol. 339*, 185−197.

BI048218B